Spectroscopic Studies on Cobalt(II)-Substituted Metallo-β-lactamase ImiS from *Aeromonas veronii* bv. *sobria*[†]

Patrick A. Crawford,[‡] Ke-Wu Yang,[‡] Narayan Sharma,[‡] Brian Bennett,[§] and Michael W. Crowder*[,‡]

Department of Chemistry and Biochemistry, 112 Hughes Hall, Miami University, Oxford, Ohio 45056, and National Biomedical EPR Center, Department of Biophysics, Medical College of Wisconsin, 8701 Watertown Plank Road, Milwaukee, Wisconsin 53226-0509

Received December 3, 2004; Revised Manuscript Received January 20, 2005

ABSTRACT: In an effort to probe the structure of a group Bb metallo-β-lactamase, Co(II)-substituted ImiS was prepared and characterized by electronic absorption, NMR, and EPR spectroscopies. ImiS containing 1 equiv of Co(II) ($Co(II)_1$-ImiS) was shown to be catalytically active. Electronic absorption studies of $Co(II)_1$-ImiS revealed the presence of two distinct features: (1) an intense sulfur to Co(II) ligand to metal charge transfer band and (2) less intense, Co(II) ligand field transitions that suggest 4-coordinate Co(II) in $Co(II)_1$-ImiS. ^{1}H NMR studies of $Co(II)_1$-ImiS suggest that one histidine, one aspartic acid, and one cysteine coordinate the metal ion in $Co(II)_1$-ImiS. The addition of a second Co(II) to $Co(II)_1$-ImiS did not result in any additional solvent-exchangeable NMR resonances, strongly suggesting that the second Co(II) does not bind to a site with histidine ligands. EPR studies reveal that the metal ion in $Co(II)_1$-ImiS is 4-coordinate and that the second Co(II) is 5/6 coordinate. Taken together, these data indicate that the catalytic site in ImiS is the consensus Zn_2 site, in which Co(II) (and by extrapolation Zn(II)) is 4-coordinate and bound by Cys221, His263, Asp120, and probably one solvent water molecule. These studies also show that the second, inhibitory metal ion does not bind to the consensus Zn_1 site and that the metal ion binds at a site significantly removed from the active site. These results give the first structural information on metallo-β-lactamase ImiS and suggest that the second metal binding site in ImiS may be targeted for inhibitors.

β-Lactamases are bacterial enzymes that hydrolyze β-lactam containing antibiotics and render the drugs ineffective. There are currently over 300 known β-lactamases, and several attempts have been made to classify these enzymes into 4 distinct groups based on molecular properties (*1*−*6*). Groups 1, 2, and 4 (or A, C, and D) are similar in that these enzymes utilize an active site serine as a nucleophile in the hydrolysis reaction. The remaining group (3 or B) is often called metallo-β-lactamases (MβL's)[1] because the enzymes require 1−2 Zn(II) for full catalytic activity (*2*, *7*−*10*). The Group B β-lactamases have been further categorized into 3 subgroups based on amino acid sequence identity and substrate affinity (*2*). The subgroup Ba β-lactamases share >23% sequence identity, exist as monomers, prefer penicillins as substrates, require 2 Zn(II) ions for full activity, and are represented by CcrA from *Bacteroides fragilis* (*11*) and β-lactamase II from *Bacillus cereus* (*12*). The subgroup Bb β-lactamases share 11% sequence identity with the Ba enzymes, prefer carbapenems as substrates, exist as a monomers, require only 1 Zn(II) for full catalytic activity, and are represented by CphA from *Aeromonas hydrophila* (*13*, *14*) and ImiS from *Aeromonas veronii* bv. *sobria* (*15*). The subgroup Bc β-lactamases have only 9 conserved amino acids, exist as tetramers, prefer penicillins and carbapenems as substrates, require 2 Zn(II) for full catalytic activity, and are represented by L1 from *Stenotrophomonas maltophilia* (*16*, *17*) and FEZ-1 from *Fluoribacter (Legionella) gormanii* (*18*). A similar grouping scheme (B1, B2, and B3) based on structural properties of the metallo-β-lactamases has recently been offered (*19*). Previous biochemical, kinetic, and inhibition studies have suggested significant structural and mechanistic differences among the different group B β-lactamases (*6*, *8*, *20*−*32*). This result suggests that one inhibitor may not be effective in treating infections caused by bacteria that produce a metallo-β-lactamase. To combat this problem, we are currently characterizing a metallo-β-lactamase from each of the group B subgroups (CcrA, ImiS, and L1) in an effort to identify common structural/mechanistic properties of the enzymes toward which a single inhibitor can be designed.

[†] This work was supported by the National Institutes of Health (AI40052 and GM40052 to M.W.C., and AI056231 to B.B.). Funds to purchase the CD spectrapolarimeter (DBI-0070206) were provided by the National Science Foundation. Funds to purchase the 500 MHz NMR spectrometer were provided by the OBoR/Hayes Investment Fund and Miami University. EPR resources were funded by the Medical College of Wisconsin and the National Institutes of Health (EB001980).

* To whom correspondence should be addressed. E-mail: crowdemw@muohio.edu. Phone: (513) 529-7274. Fax: (513) 529-5715.

[‡] Miami University.

[§] Medical College of Wisconsin.

[1] Abbreviations: CcrA, metallo-β-lactamase from *Bacteroides fragilis*; CphA, metallo-β-lactamase from *Aeromonas hydrophila*; FEZ-1, metallo-β-lactamase from *Fluoribacter gormanii*; HEPES, 4-(2-hydroxymethyl)-1-piperazineethanesulfonic acid; ICP-AES, inductively coupled plasma with atomic emission spectroscopy detection; ImiS, metallo-β-lactamase from *Aeromonas sobria*; IPTG, isopropyl-β-D-thiogalactopyranoside; L1, metallo-β-lactamase from *Stenotrophomonas maltophilia*; LB, Luria-Bertani; MβL, metallo-β-lactamase; RFQ, rapid freeze quench.

10.1021/bi047463s CCC: $30.25
Published on Web 03/08/2005

One part of our approach is the use of rapid freeze quench methods in conjunction with EPR and EXAFS to probe the structure about the metal ions (Co(II)-substituted) during the early stages of the hydrolytic mechanism.

While there is considerable information available on the subgroup Ba and Bc metallo-β-lactamases, such as X-ray crystal structures (*17*, *33*−*35*) and spectroscopic, mechanistic, (*11*, *12*, *21*, *29*, *36*−*40*), and computational studies (*41*−*48*), there is much less known about the structure and mechanism of any of the subgroup Bb enzymes. UV−vis and EXAFS spectroscopic studies have been reported on Co(II)-substituted CphA from *A. hydrophila*, and these studies suggested that the tightly bound Co(II) (Zn(II)) is coordinated by 2 histidines, 1 cysteine, and 1 additional N/O ligand (*14*). By comparing the structures and amino acid sequences of the X-ray crystallographically characterized metallo-β-lactamases with the amino acid sequence of CphA, it is evident that the spectroscopically predicted metal binding site is unique among the metallo-β-lactamases and requires that ligands from the consensus Zn_1 and Zn_2 sites contribute ligands to one Co(II) in CphA. In order to probe the mechanism of a subgroup Bb metallo-β-lactamase using future rapid freeze quench (RFQ) spectroscopic studies, it is essential that the spectroscopic properties of the resting enzyme, the Co(II)-substituted form in this case, be characterized. This work describes our work on metallo-β-lactamase ImiS (*15*, *49*), a subgroup Bb enzyme from *A. veronii* bv. *sobria*.

EXPERIMENTAL PROCEDURES

Preparation of Co(II)-Substituted ImiS. The overexpression plasmid, pET26b-ImiS, was used to transform BL21(DE3) *Escherichia coli* cells (*50*). A 10 mL overnight culture of these cells in LB (Luria-Bertani) medium was used to inoculate 4 × 1 L of LB medium containing 25 μg/mL kanamycin and 29 μg/mL $ZnSO_4 \cdot 7H_2O$. The cells were allowed to grow at 37 °C with shaking until the cells reached an optical density at 600 nm of 0.6−0.8. Protein production was induced with 1 mM isopropyl-β-D-thiogalactopyranoside (IPTG), and the cells were shaken at 37 °C for 3 h. The cells were collected by centrifugation (15 min at 9506*g*) and resuspended in 30 mL of 50 mM Tris, pH 7.0, containing 500 mM NaCl. The cells were ruptured by two passages through a French press at 16000 lb/in.^{2}, and the cell debris was separated by centrifugation (30 min at 23419*g*). The cleared supernatant was dialyzed versus 50 mM Tris, pH 7.0, overnight at 4 °C, centrifuged to remove insoluble matter, and loaded onto an equilibrated Q-Sepharose column (1.5 by 12 cm with 25 mL bed volume). Bound proteins were eluted with a 0 to 500 mM NaCl gradient in 50 mM Tris, pH 7.0, at 2 mL/min. Fractions (8 mL) containing ImiS were pooled and concentrated with an Amicon ultrafiltration cell equipped with a YM-10 membrane. Protein purity was ascertained by sodium dodecyl sulfate (SDS) polyacrylamide gel electrophoresis.

Apo-ImiS was prepared by four dialysis steps of recombinant ImiS (60−100 mg) against a 300-fold excess of 15 mM HEPES (4-(2-hydroxymethyl)-1-piperazineethanesulfonic acid), pH 6.5, containing 10 mM EDTA (12 h each dialysis at 4 °C). The EDTA was removed completely by three dialysis steps against the same buffer containing 150 mM sodium chloride, followed by passage through a 1.5 × 68-cm column of Sephadex G-25 (bed volume 120 mL), equilibrated with 15 mM HEPES, pH 6.5, containing 100 mM NaCl (*51*). The column flow rate was adjusted to 1 mL/min, and 6 mL of fractions were collected and monitored by absorbance at 280 nm. Column fractions containing ImiS were pooled and concentrated using ultrafiltration, as described above. ICP-AES was used to demonstrate that the Zn(II) had been removed from the enzyme samples.

To prepare Co(II)-substituted ImiS, 1−2 molar equiv of $CoCl_2$ were added directly to solutions of apo-ImiS, and the enzyme samples turned blue in color within 1 min. The samples were incubated on ice for 1 h, dialyzed versus 2 × 1 L of freshly chelexed 50 mM HEPES, pH 6.5, at 4 °C over 6 h, concentrated, and then used in spectroscopic studies. The activity and blue color of Co(II)-ImiS persisted at least for one month at 4 °C. ^{1}H NMR spectra were used to demonstrate if the EDTA had been completely removed from the samples (*51*).

Steady-State Kinetics. Steady-state kinetic studies were carried out in 50 mM Tris buffer, pH 7.0, on a Hewlett-Packard 5480A UV−vis spectrophotometer, using an Isotemp circulator to maintain the reactions at 25 °C. The errors are reported as standard deviations (σ_{n-1}) from multiple kinetic trials (*16*).

Electronic Absorption Spectra of Co(II)-Substituted ImiS. Electronic absorption spectra were obtained on a Hewlett-Packard 5480A spectrophotometer. Background spectra of apo-ImiS were used to generate difference spectra of the Co(II)-substituted samples.

Circular Dichroism Spectroscopy. Circular dichroism samples were prepared by dialyzing the purified enzyme samples versus 3 × 2 L of 5 mM phosphate buffer, pH 7.0, over 6 h. The samples were diluted with final dialysis buffer to ∼75 μg/mL. A JASCO J-810 CD spectropolarimeter operating at 25 °C was used to collect CD spectra (*16*, *24*).

NMR Spectra of Co(II)-Substituted ImiS. NMR spectra were collected on a Bruker Avance 500 NMR spectrometer operating at 500.13 MHz, 298 K and a magnetic field of 11.7 T. The spectra were obtained by using a modified presaturation pulse sequence (zgpr) for water suppression and the following parameters: recycle delay (AQ), 41 ms; sweep width, 400 ppm; receiver gain, 128; line broadening, 80 Hz. The samples for NMR studies were made by concentrating apo-ImiS using an Amicon equipped with a YM-10 membrane or a Centricon-10 to final concentrations of ca. 1.1 mM and adding corresponding equivalent $CoCl_2$. The sample volumes were approximately 0.4 mL. Protein chemical shifts were calibrated by assigning the H_2O signal the value of 4.70 ppm at 298 K.

EPR Spectra of Co(II)-Substituted ImiS. EPR spectra were recorded at 9.6330 ± 0.0005 GHz using a Bruker EleXsys E-500-10W/12 EPR spectrometer equipped with a SuperX 90 dB X-band microwave bridge, an ER-4116DM dual mode TE_{102}/TE_{012} resonant cavity, an Oxford Instruments ESR900 helium flow cryostat, and an Oxford Instruments ITC502 temperature controller. EPR simulations were carried out by matrix diagonalization using XSophe v.1.1.2 (Bruker Biospin GmbH (*52*)). Parameters were fitted to the spin Hamltonian $H = \beta \mathbf{g \cdot H \cdot S} + \mathbf{S \cdot D \cdot S} + \mathbf{S \cdot A \cdot I}$, explicitly assuming $S = {}^3/_2$ and using experimentally measured temperatures (±0.1 K) and microwave frequencies (±0.00001 GHz). Under the spin

Hamiltonian formalism employed by XSophe, $D > 0$ corresponds to an $M_S = |\pm^1/_2\rangle$ ground state and $D < 0$ corresponds to an $M_S = |\pm^3/_2\rangle$ ground state. A *g*-strain line width model was employed and, where ^{59}Co hyperfine structure was observed, *A*-strain was also included (*53*).

Rapid passage and/or saturation effects are often overlooked in EPR studies of high-spin Co(II). These effects can be responsible for either relatively minor degrees of misinterpretation of the signals, such as inaccurate spin Hamiltonian parameters, or major misinterpretation, such as the incorrect assignment of the Kramers doublet in which the transition occurs. The latter is a consequence of the absorption-like appearance of transitions under rapid passage conditions that, under ideal conditions, are actually derivative-shaped features, and can lead to incorrect geometrical interpretation of the system. In the present study, the deconvolution of individual species and the use of computer simulation were essential in facilitating the identification of conditions under which saturation and/or rapid passage effects were negligible. For each species, at least one set of conditions was identified and employed under which that species exhibited (i) square-root (microwave power) dependence and (ii) equal integrated intensity above and below the baseline (for $M_S = |\pm^1/_2\rangle$ signals). Extensive studies of the microwave power, temperature, and field modulation depenedencies of some signals were carried out. Rapid passage effects on some of the signals were characterized. These studies revealed significant differences in relaxation behavior between some signals but provided little additional structural information on the major species, and detailed consideration of these data was thus deemed outside the scope of the present work.

RESULTS

Characteristics of Apo-ImiS and Co(II)-Substituted ImiS. Apo-ImiS was found to contain < 0.05 equiv of Zn(II) and exhibit a steady-state k_{cat} of <0.31 s^{-1}, less than 0.1% of native ImiS, when using imipenem as substrate. CD spectra showed that apo-ImiS maintains structural features consistent with those of the as-isolated ImiS (*50*): 19% α-helix, 47% *β*-character, and 33% unstructured (data not shown). When 1 equiv of Co(II) was added to apo-ImiS ($Co(II)_1$-ImiS), the resulting enzyme turned light blue in color. Steady-state kinetic studies revealed that $Co(II)_1$-ImiS is catalytically active with a k_{cat} of 255 ± 16 s^{-1} and a K_M of 99 ± 12 μM, when using imipenem as the substrate. Steady-state kinetic studies on $Co(II)_2$-ImiS revealed a 5-fold reduction in k_{cat} and no change in K_m, which is in excellent agreement with previous studies on CphA (*14*, *54*). These numbers are similar to those previously reported on the $Zn(II)_1$-ImiS (k_{cat} = 315 s^{-1} and K_m = 46 μM) (*50*). CD spectra (not shown) were identical to those of as-isolated $Zn(II)_1$-ImiS (*50*) and apo-ImiS.

Electronic Absorption Spectra of Co(II)-Substituted ImiS. Electronic absorption spectra of ImiS containing between 1 and 3 equiv of Co(II) are shown in Figure 1. Upon addition of up to 1 equiv Co(II), an absorption band that was centered at 340 nm and that exhibited ϵ_{340} = 950 M^{-1} cm^{-1} (per ImiS) was observed. Less intense features were also evident, with ϵ_{550} = 306 M^{-1} cm^{-1} and ϵ_{600} = 392 M^{-1} cm^{-1}. Upon further addition of up to 2 equiv Co(II), the only change was a slight increase in the molar absorptivity of the lower energy absorption bands to ϵ_{550} = 367 M^{-1} cm^{-1} and ϵ_{600} = 416 M^{-1} cm^{-1}.

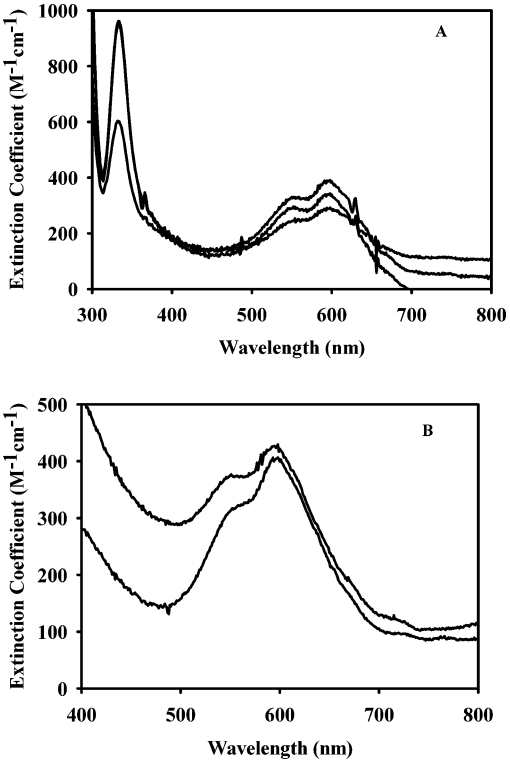

FIGURE 1: Electronic spectra of ImiS containing Co(II). (A) Difference spectra for ImiS containing 1 equiv of Co(II) (bottom curve), 2 equiv of Co(II) (middle curve), and 3 equiv of Co(II) (top curve). (B) Spectra for ImiS containing 1 equiv of Co(II) (bottom curve) and 2 equiv of Co(II) (top curve). Difference spectra were generated by subtracting the spectrum of apo-ImiS from the experimental spectra.

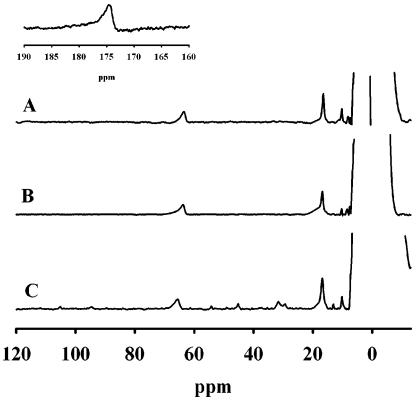

FIGURE 2: 500 MHz, ^{1}H NMR spectra of Co(II)-substituted ImiS. (A) Spectrum of 1.1 mM ImiS containing 1 equiv of Co(II). (B) Spectrum of 1.1 mM ImiS containing 2 equiv of Co(II). (C) Spectrum of 1.1 mM ImiS containing 10 equiv of Co(II). Inset: Peak at 175 ppm in spectrum of 1.1 mM ImiS containing 1 equiv of Co(II). The buffer for these samples was 50 mM Hepes, pH 7.0, in 10% D_2O. The experimental parameters were as follows: temperature, 298 K; FID resolution, 6.10 Hz; acquisition time, 41 ms; sweep width, 400 ppm; receiver gain, 128; line broadening, 80 Hz.

^{1}H NMR Spectra of Co(II)-Substituted ImiS. The ^{1}H NMR spectrum of $Co(II)_1$-ImiS reveals three relatively sharp proton resonances between 10 and 80 ppm (Figure 2) and one broad resonance at 175 ppm (Figure 2, inset). A spectrum of the same sample in 90% D_2O revealed that only the signal at

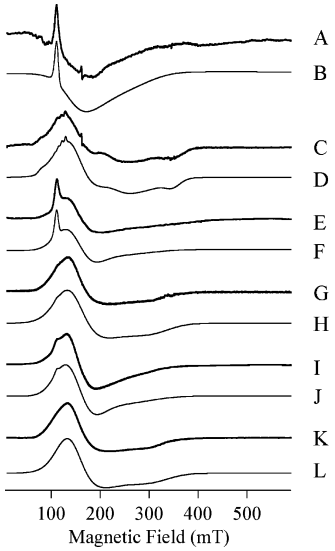

FIGURE 3: EPR spectra of ImiS upon addition of Co(II). EPR spectra of ImiS were recorded after incubation with 0.5 (A and C), 1.0 (E and G), and 2.0 (I and K) equiv of Co(II). Spectra were recorded using 1.06 mT, 100 kHz field modulation with the following temperatures and microwave powers: 5 K, 63 mW (A); 12 K, 2 mW (C); 5 K, 160 mW (E and I); 16 K, 0.5 mW (G and K). Traces B, D, F, H, J, and L are computer simulations of spectra A, C, E, G, I, and K, respectively. The simulations B, D, F, H, and J are composed of admixtures of individual species shown in Figure 4, and the EPR parameters are given in the caption to Figure 4. Trace L is a simulation of K assuming a single species; the simulation is reproduced (2F) and the parameters given in Figure 4 for clarity. Trace 3B is an admixture of traces 4B and 4J; 4J is inverted. Trace 3D is an admixture of traces 4D (25%) and 4F (75%). Traces 3F and 3J are admixtures of traces 4B and 4H; 3F contains twice the relative amount of 4B than does 3J. Trace 3H is an admixture of traces 4B and 4F.

63 ppm is solvent-exchangeable (see figure in Supporting Information). Therefore, we assign this resonance to an NH proton of a Co(II)-bound histidine (*55*). The resonance at 19 ppm is in the range corresponding to β-CH_2 protons of a Co(II)-bound Asp (*56*, *57*). The narrow signal at 13 ppm is tentatively assigned to β-CH_2 protons of the Co(II)-bound histidine. Similar assignments were reported on Co(II)-substituted alcohol dehydrogenase (*58*) and Co(II)-substituted carbonic anhydrase (*59*). The ratio of NMR peak integrations of the peaks at 63 and 19 ppm is 1:2, respectively, for Co-$(II)_1$-ImiS.

NMR spectra were also collected for Co(II)-substituted ImiS samples containing 2, 4, and 10 equiv of Co(II). In the spectrum for $Co(II)_2$-ImiS, no other proton resonances were observed in the region of 10−100 ppm, suggesting that the second equivalent of Co(II) does not coordinate His residues. Therefore, NMR spectra of Co(II)-substituted ImiS containing 4 and 10 equiv of Co(II) were collected, and several new peaks in the region of 10−70 ppm were observed. However, none of these newly observed resonances were solvent-exchangeable.

EPR Spectra of Co(II)-Substituted ImiS. EPR spectra of Co(II)-substituted ImiS were recorded under various conditions, and a range of spectra from which all of the EPR-detectable species of Co(II)-substituted ImiS could be extracted is presented in Figure 3. Each of these experimental EPR spectra could be simulated as being due to either one or two distinct chemical species. The EPR signals from these distinct chemical species were isolated from the experimentally observed spectra shown in Figure 3 by difference techniques, and the EPR signals due to these species and their simulations are shown in Figure 4.

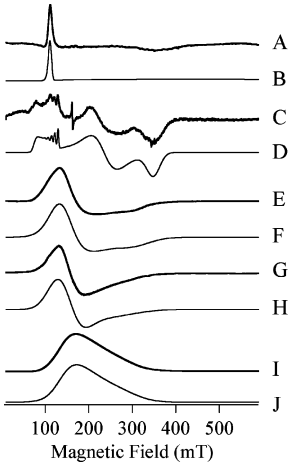

FIGURE 4: Individual EPR-detectable species of ImiS. Traces A, C, E, and G are EPR signals proposed to be due to single chemical species and were obtained by difference from the experimentally observed spectrum shown in Figure 3E. Traces B, D, F, and H are computer simulations of A, C, E, and G, respectively, and were obtained assuming a single magnetic species in each case. Traces I and J were generated by integration of traces 3K and 3L, respectively. Species A was obtained by subtraction of I (inverted) from trace 3A. Trace B is a simulation assuming $S = {}^3/_2$, $M_S = |\pm{}^3/_2\rangle$, $g_{\mathrm{eff}(z)} = 6.2$, corresponding to $2.27 \geq g_{\mathrm{real}(z)} \geq 2.07$ for $|D| \gg |g\beta BS|$. Species C was obtained by subtraction of trace 3K from 3C. Simulation D assumed $S = {}^3/_2$, $M_S = |\pm{}^1/_2\rangle$, $g_\perp = 2.50$, $g_{||} = 2.44$, $D = 50\ \mathrm{cm}^{-1}$, $E/D = 0.27$, $A_z(^{59}\mathrm{Co}) = 8.6 \times 10^{-3}\ \mathrm{cm}^{-1}$. Species E was generated by subtraction of A from trace 3K. Simulation F assumed $S = {}^3/_2$, $M_S = |\pm{}^1/_2\rangle$, $g_\perp = 2.22$, $g_{||} = 2.27$, $D = 50\ \mathrm{cm}^{-1}$, $E/D = 0.05$. Trace G was generated by subtraction of A from trace 3I. Simulation H assumed $S = {}^3/_2$, $M_S = |\pm{}^1/_2\rangle$, $g_\perp = 2.32$, $g_{||} = 2.50$, $D = 50\ \mathrm{cm}^{-1}$, $E/D = 0$.

EPR spectra of $Co(II)_{0.5}$-ImiS were highly dependent upon the recording conditions. At low temperature and high microwave power (5 K, 63 mW), a spectrum (Figure 3A) was observed that exhibited a sharp spike at 111.6 mT ($g_{\mathrm{eff}} = 6.2$) and an underlying broad resonance. Given the EPR conditions employed and given the clear dissimilarity of the broad signal to a well-formed, field-modulated, phase-sensitive-detected EPR signal, an attempt at quantitation of these signals was not appropriate. At higher temperature and lower microwave power (i.e. nonsaturating conditions: 12 K, 2 mW), a complex signal (Figure 3C) was observed that was deconvoluted into two distinct species. A rhombic species with some resolved hyperfine splitting (Figure 4C) was simulated (Figure 4D) with spin Hamiltonian parameters of $M_S = |\pm{}^1/_2\rangle$, $g_\perp = 2.50$, $g_{||} = 2.44$, $D \gg g\beta BS$, $E/D = 0.27$, and $A_z(^{59}\mathrm{Co}) = 8.6 \times 10^{-3}\ \mathrm{cm}^{-1}$. This species accounted for 25% of the total spins observable under these conditions, corresponding to only 5% of the added Co(II). A second, axial component, corresponding to 75% of the observable spins but only 15% of the added Co(II), was simulated assuming $M_S = |\pm{}^1/_2\rangle$, $g_\perp = 2.22$, $g_{||} = 2.27$, $D \gg g\beta BS$, and $E/D = 0.05$ (Figure 4F). The composite simulation (Figure 3D) reproduced the experimental spectrum (Figure 3C) well, but this spectrum accounted for only 20% of the added Co(II). If the very sharp signal detected at low temperature and high power represents the balance of Co-(II), then this signal may account for 80% of the added Co-(II).

Upon incubation of ImiS with 1 equiv of Co(II), a spectrum (Figure 3E) was observed at 5 K and 160 mW that still contained the sharp signal at $g_{eff} = 6.2$, which was observed with $Co(II)_{0.5}$-ImiS. However, instead of, or in addition to, the broad trough-like feature observed in the high power, low temperature spectrum of $Co(II)_{0.5}$-ImiS, a more intense axial feature was evident. At 16 K and 0.5 mW, the sharp signal was only evident as a shoulder on the now unsaturated and well-resolved axial signal (Figure 3G). Taken together, the spectra 3E and 3G show clearly different relaxation behaviors for the two axial species. The very sharp signal is barely observable under conditions that are nonsaturating for the axial signal. However, the axial signal did not exhibit the distortion observed in spectrum 3A, and integration, corrected for temperature and $(power)^{1/2}$, indicated that the axial signal in 3E exhibits 78% of the expected intensity for an unsaturated signal. The very sharp signal is very difficult to quantify as the true positions of the other two resonance positions are unknown. However, simulations with various parameters produce spectra that, when doubly integrated, suggest that the sharp signal could account for up to 85% of the spin density. In support of this estimate, quantitation of the axial component recorded under nonsaturating conditions (Figure 4E) indicates that it accounts for only 10% of the added Co(II). Thus, the very sharp signal is the predominant paramagnetic species in terms of number of spins. These observations serve to highlight the importance of recording spectra under multiple conditions and to illustrate that the appearance of spectra can be deceptive when one is considering the spin concentrations of contributory species.

Upon further addition of Co(II) up to 2 equiv, the axial component, evident in the spectra of $Co(II)_1$-ImiS (Figures 3E and 3G), exhibited a marked increase in intensity, corresponding to the additional 1 equiv of added Co(II). The axial component, which was observed both at high power, low temperature (160 mW, 5 K) and at low power, high temperature (0.5 mW, 16 K) conditions, was isolated by difference methods and simulated. Under nonsaturating conditions, the signal (Figure 4E) was simulated (Figure 4F) assuming $M_S = |\pm^1/_2\rangle$, $g_\perp = 2.22$, $g_{||} = 2.27$, $D \gg g\beta BS$, and $E/D = 0.05$. At 5 K and 160 mW, the signal (Figure 4G) was partially saturated, which was evident from the higher area below the baseline than above it. In addition, some of the spectral features had shifted slightly, resulting in different parameters for the simulation of spectra recorded under these conditions (Figure 4H). The parameters from the simulation of the axial components of the spectra for $Co(II)_1$- and $Co(II)_2$-ImiS recorded at 5 K and 160 mW do not represent accurate spin Hamiltonian parameters, though the simulation was useful in constructing the simulations (Figure 3F and 3J) of the experimental spectra (Figure 3E and 3I).

DISCUSSION

Structural studies on Zn(II)-containing metalloproteins are limited by the fact that Zn(II) is diamagnetic, and therefore, metal binding sites containing Zn(II) cannot be characterized by common optical and magnetic techniques including electronic absorption spectrophotometry, magnetic circular dichroism, paramagnetic ^{1}H NMR, and EPR spectroscopies. Fortunately, spectroscopically active Co(II) can often replace Zn(II) in these proteins to yield a catalytically active enzyme with a structurally homologous active metal center. Co(II)-substituted ImiS was prepared by the direct addition method (*60*), and the resulting enzyme exhibited significant catalytic activity and a similar secondary structure as the native enzyme. UV−vis, paramagnetic ^{1}H NMR, and EPR studies were conducted on Co(II)-substituted ImiS in an effort to probe the electronic structure of the metal binding site.

Electronic absorption spectrophotometry on Co(II)-substituted ImiS revealed two distinct sets of absorption bands. The intense feature at 340 nm is consistent with a Cys→Co(II) ligand-to-metal charge transfer (LMCT) as has been seen in other Co(II) proteins (*12*, *36*, *38*), including Co(II)-CphA ($\epsilon_{325} = 530$ M^{-1} cm^{-1} at pH 7.5) (*61*). This result strongly suggests that the first metal binding site for ImiS contains a cysteine ligand. The broad features between 500 and 650 nm are attributable to ligand field transitions (Figure 1B). Often ligand field transitions of high-spin Co(II) can be correlated with the coordination number of the metal ion. The intensities of four-coordinate (tetrahedral) Co(II) are typically >300 M^{-1} cm^{-1}, of five-coordinate Co(II) centers are ca. 100−150 M^{-1} cm^{-1}, and of six-coordinate (octahedral) Co(II) centers are <30 M^{-1} cm^{-1} (*62*). The coordination number (geometry)/intensities are due to increased pd orbital mixing of metal orbitals and increased Laporte-character in the transitions. In the spectrum of $Co(II)_1$-ImiS, the extinction coefficients of the ligand field transitions are >300 M^{-1} cm^{-1}. These data strongly suggest tetrahedral coordination of Co(II) in $Co(II)_1$-ImiS (*62*). The addition of a second equivalent of Co(II) results in small increases in the intensities of the ligand field transitions: $\Delta\epsilon_{550} = 61$ M^{-1} cm^{-1} and $\Delta\epsilon_{600} = 24$ M^{-1} cm^{-1} (per ImiS). These increases are consistent with the second equivalent of Co(II) being five- or six-coordinate.

Paramagnetic ^{1}H NMR spectroscopy has been used previously to probe the metal binding sites of Co(II)-substituted enzymes, in particular those with histidine ligands (*59*, *63*−*65*). The NMR spectrum of $Co(II)_1$-ImiS revealed three sharp signals between 19 and 70 ppm and a broad peak at 175 ppm. The peak at 175 ppm can be assigned to β-CH_2 protons on a Co(II)-coordinated cysteine (*12*, *57*, *66*). This assignment strongly supports the prediction, from optical absorption data, of cysteine-derived sulfur ligation of Co(II) in $Co(II)_1$-ImiS. These data further suggest that the first Co(II) binds to the consensus Zn_2 binding site in ImiS that was identified by sequence homology with X-ray crystallographically characterized β-lactamases. The observation of only one solvent-exchangeable resonance (63 ppm), which is assigned to a histidine ligand (probably His263), supports this proposal. In addition, it is likely that the peak at 19 ppm results from methylene protons on a Co(II)-coordinated Asp residue (Asp120). Thus, both NMR and spectrophotometric studies strongly suggest that the catalytic site in Co(II)-substituted ImiS is the Zn_2 site.

A second "consensus" site that was identified in ImiS consists of an asparagine and two histidine residues, and is termed the Zn_1 site. However, the NMR spectra of ImiS with more than two or more equivalents of Co(II) provide no evidence for binding of Co(II) to the Zn_1 site in ImiS; two solvent-exchangeable peaks that would have been expected to indicate binding to the Zn_1 site were not observed. Interestingly, kinetic studies have demonstrated that a second

equivalent of Zn(II) is a noncompetitive inhibitor of both ImiS (*50*) and the related enzyme CphA (*13*). These observations are consistent with binding of the second equivalent of Zn(II) to a site distinct from the active site, and support the indication from NMR data that the consensus Zn_1 site is not actually the binding site for a second metal ion in ImiS.

EPR spectroscopy unambiguously identified two distinct species of Co(II) associated with ImiS. The first species, with $g_{\mathrm{eff}(z)} = 6.2$ (Figure 4A), can be readily assigned to $M_S = |\pm^3/_2\rangle$ and thus to tetrahedral Co(II). This tetrahedral species is the predominant species in $Co(II)_{0.5}$-ImiS, and likely accounts for 80% of the added Co(II). The signal increases in intensity upon addition of 1.0 equiv of Co(II), accounting for up to 90% of the added Co(II), and no further increase in the intensity can be observed in the spectrum of $Co(II)_2$-ImiS. This result is entirely consistent with the prediction of tetrahedral Co(II) in the first metal binding site. Real *g* values and values for *E*/*D* could not be accurately determined ($2.27 \geq g_{\mathrm{real}(z)} \geq 2.07$ for $|D| \gg |g\beta BS|$), and further structural information on the basis of electronic symmetry is not forthcoming. Nevertheless, both the form and the relaxation properties of the signal bear a striking resemblance to those from the Co(II)-substituted aminopeptidase from *Vibrio proteolyticus* (reclassified from *Aeromonas proteolytica*) in complexation with thiol-containing inhibitors (*66*, *67*), and these observations provide some support for the proposal, from optical and NMR spectroscopies, that the tetrahedral site provides a sulfur ligand to the metal ion.

The second species that is clearly and quantitatively associated with ImiS is the axial signal with $M_S = |\pm^1/_2\rangle$, $g_\perp = 2.22$, $g_{||} = 2.27$, $D = 50\ \mathrm{cm}^{-1}$, and $E/D = 0.05$. This signal is distinguishable by its resistance to saturation from the axial signal from $Co(II)_{0.5}$-ImiS and indeed is undetectable in the spectrum of $Co(II)_{0.5}$-ImiS. The signal accounts for only 0.1 equiv of Co(II) in the spectrum of $Co(II)_1$-ImiS but accounts for 1 equiv of Co(II) in the spectrum of $Co(II)_2$-ImiS. The EPR data concur with the electronic absorption spectra in indicating either 5-fold or 6-fold coordination of this Co(II) ion, with no sulfur coordination.

It is noteworthy that computer simulation of the spectrum of $Co(II)_2$-ImiS indicates that the very sharp signal is still exhibited, and at the same intensity at which it is present in the spectrum of $Co(II)_1$-ImiS. The temperature dependence of this signal is indistinguishable in $Co(II)_1$-ImiS and $Co(II)_2$-ImiS. Of further note, the axial component of $Co(II)_2$-ImiS also accounts for 1 equiv of Co(II). The EPR data, taken together, clearly show that ImiS initially binds 1 equiv of Co(II) in a tetrahedral site, with 80−90% selectivity, and the data are strongly supported by electronic absorption spectrophotometry. EPR data are consistent with this Co(II) ion possessing a sulfur ligand, in support of the more definitive electronic absorption and NMR data. Upon saturation of one binding site with 1 equiv of Co(II), ImiS binds a second, five- or six-coordinate Co(II) ion in a distinct site. The two Co(II) ions continue to exhibit EPR signals with line shapes, intensities, and relaxation properties consistent with their being magnetically isolated, mononuclear Co(II) signals; there is no evidence for any change in the properties of the very sharp signal, due to the first Co(II) ion, upon the binding of the second Co(II). The signal due to the second Co(II) is readily quantitated and accounts for 1 equiv of Co(II). Matrix diagonalization simulations (not shown) of interactions of the two Co(II) ions place a lower limit of 7 Å on the distance between the two Co(II) ions and an upper limit of 0.02 cm^{-1} for any isotropic exchange coupling. Thus, the two Co(II) binding sites are distinct in terms of geometry and binding affinity, and they are physically separated from each other, i.e. they do not constitute a dinuclear site.

The assignment of the EPR signals that are relevant to the structure and function of ImiS is essentially straightforward, following directly from the deconvolution, characterization, and quantitation of the distinct species that make up the experimental spectra. However, this may not be immediately obvious from the experimental data; other minor species were observed that complicated the EPR spectra. In order to characterize, quantitate, and ultimately rule out these species as being relevant to the structure and function of ImiS, these signals were analyzed in a manner analogous to that employed for the major signals. One species, clearly identified in $Co(II)_{0.5}$-ImiS and corresponding to 0.025 equiv of Co(II), exhibited the spin Hamiltonian parameters: $M_S = |\pm^1/_2\rangle$, $g_\perp = 2.50$, $g_{||} = 2.44$, $A(^{59}\mathrm{Co}) = 8.6 \times 10^{-3}\ \mathrm{cm}^{-1}$, and $E/D = 0.27$ with $D \gg g\beta BS$. The $M_S = |\pm^1/_2\rangle$ manifold corresponds to either five- or six-coordinate Co(II), and the high value of *E*/*D* and the low *g*-strain, indicated by the resolved ^{59}Co hyperfine lines, are both indicative of a five- or six-coordinated Co(II) ion, highly distorted from ideal octahedral geometry (*68*). This signal accounted for only a very small amount of the Co(II) in $Co(II)_{0.5}$-ImiS and could not be detected at all in the spectra of $Co(II)_1$-ImiS or $Co(II)_2$-ImiS; its origin is unclear, and it was not investigated further.

The other minor species that was observed, again only visible in the spectrum of $Co(II)_{0.5}$-ImiS, was almost indistinguishable from the axial component of $Co(II)_2$-ImiS when recorded under nonsaturating conditions. The signal accounted for only 0.075 equiv of Co(II) in the spectrum of $Co(II)_{0.5}$-ImiS. Despite the similarity to the well-characterized axial component of $Co(II)_2$-ImiS, this axial signal from $Co(II)_{0.5}$-ImiS exhibited relaxation behavior very different from that from $Co(II)_2$-ImiS. Whereas the form of the predominant axial signal from $Co(II)_2$-ImiS (also visible in $Co(II)_1$-ImiS, though accounting for only 0.1 equiv of Co(II)) was only slightly affected by low temperatures and high powers, and exhibited essentially Curie law temperature dependence at moderate microwave powers, the axial signal from $Co(II)_{0.5}$-ImiS exhibited marked rapid-passage effects at low temperatures. There was no firm evidence for the presence of this signal in the spectra of $Co(II)_1$-ImiS or $Co(II)_2$-ImiS, and no investigation of its origin was undertaken in view of the very small amount of Co(II) that the signal represents.

The spectroscopic studies reported herein strongly suggest that the catalytic, tight-binding site in ImiS is the consensus Zn_2 site. By comparing the sequences of other metallo-β-lactamases, we predict that this metal binding site is made up of Cys221, His263, and Asp120 and that there is one solvent water molecule bound (Figure 5). This site differs from that previously predicted by spectroscopic studies for the similar subgroup Bb metallo-β-lactamase CphA (*14*). This work does, however, support recent mutagenesis studies on CphA that suggested that Cys221 is a metal binding ligand to Zn_1 (*69*). In addition, a recent crystal structure of CphA (*70*), reported during the time that this present manuscript

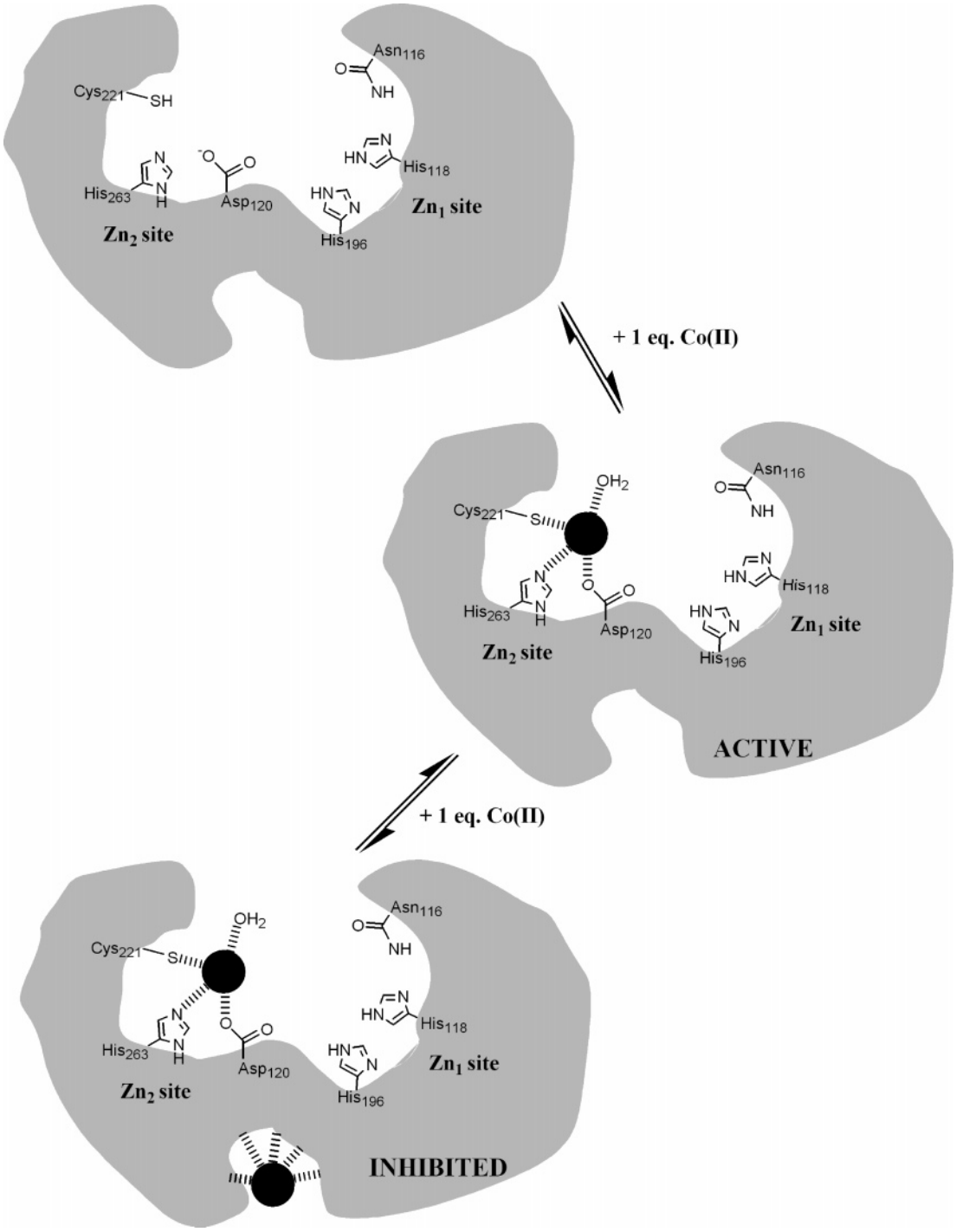

FIGURE 5: Proposed metal binding sites in ImiS.

was reviewed, shows that Zn(II) binds to Cys221, His263, and Asp120, which is the exact site predicted by our spectroscopic studies. It is unclear why the previous spectroscopic studies on CphA (*14*) predicted a different metal binding site; however, it is possible that the freeze-drying of the CphA samples used in the EXAFS studies may have affected the structure of the enzyme.

The identification of the true metal binding site in the subgroup Bb enzymes is important for future inhibitor design efforts. It is not clear whether the Zn_2 site is the catalytic site in the other metallo-β-lactamases; however, β-lactamase II has been shown to be catalytically active with metal bound in the Zn_1 site. These results offer insight into how metallo-β-lactamases have evolved to be active as mononuclear and dinuclear Zn(II)-containing enzymes. These studies also demonstrate that the second, inhibitory metal binding site in ImiS (and probably CphA) is not the consensus Zn_1 site, in contrast to previous work (*69*). This result suggests that there is a remote binding site in ImiS that can affect the activity of the enzyme; it is conceivable that this binding site could be targeted for inhibitors.

CONCLUSIONS

ImiS is a metallo-β-lactamase that contains two amino acid sequence motifs that appear to code for adjacent metal binding sites, Zn_1 and Zn_2. ImiS binds up to 2 equiv of Zn(II) or Co(II) but is maximally active with only 1 equiv of metal ion. EPR, electronic absorption, and NMR spec-

troscopies show that the first metal binds to a site that furnishes a tetrahedral coordination sphere that includes a cysteine-derived sulfur ligand and a histidine side chain. The Zn_2 site contains both a catalytically essential cysteine residue and a histidine residue and it is, therefore, proposed that the Zn_2 site binds the first equivalent of added metal ion and constitutes the hydrolytically active site of ImiS. The Zn_1 site contains an asparagine and two histidine residues, and is adjacent to the Zn_2 site. However, NMR studies do not detect any histidine coordination to a second equivalent of added Co(II). The addition of a second equivalent of metal ion competitively inhibits ImiS, suggesting a binding site remote from Zn_2, and EPR indicates that a second Co(II) ion binds in a five- or six-coordinate site, and is at least 7 Å distant from the first Co(II) ion. Thus, the Zn_1 site appears to have no catalytic or metal-binding role in ImiS, whereas Zn_2 binds the hydrolytic metal ion, and a third, as yet uncharacterized site binds metal ions with a lower affinity than Zn_2 with concomitant inhibition of ImiS.

SUPPORTING INFORMATION AVAILABLE

^{1}H NMR spectra of $Co(II)_1$-ImiS in D_2O, apo-ImiS, and $Co(II)_1$-ImiS. This material is available free of charge via the Internet at http://pubs.acs.org.

REFERENCES

1. Ambler, R. P. (1980) The Structure of β-Lactamases, *Philos. Trans. R. Soc. London, Ser. B 289*, 321−331.
2. Bush, K. (1998) Metallo-β-Lactamases: A Class Apart, *Clin. Infect. Dis. 27* (Suppl. 1), S-48−53.
3. Bush, K. (1989) Classification of β-lactmases: Groups 1, 2a, 2b, and 2b′, *Antimicrob. Agents Chemother. 33*, 264−270.
4. Bush, K. (1989) Classification of β-lactmases: Groups 2c, 2d, 2e, 3 and 4, *Antimicrob. Agents Chemother. 33*, 271−276.
5. Bush, K., Jacoby, G. A., and Medeiros, A. A. (1995) A Functional Classification Scheme for β-lactmases and Its Correlation with Molecular Structure, *Antimicrob. Agents Chemother. 39*, 1211−1233.
6. Rasmussen, B. A., and Bush, K. (1997) Carbapenem-Hydrolyzing β-Lactamases, *Antimicrob. Agents Chemother. 41*, 223−232.
7. Cricco, J. A., Orellano, E. G., Rasia, R. M., Ceccarelli, E. A., and Vila, A. J. (1999) Metallo-β-Lactamases: Does it Take Two to Tango?, *Coord. Chem. Rev. 190*−*192*, 519−535.
8. Crowder, M. W., and Walsh, T. R. (1999) Metallo-β-Lactamases: Structure and Function, *Res. Signpost 3*, 105−132.
9. Payne, D. J. (1993) Metallo-β-lactamases−A New Therapeutic Challenge, *J. Med. Microbiol. 39*, 93−99.
10. Wang, Z., Fast, W., Valentine, A. M., and Benkovic, S. J. (1999) Metallo-β-Lactamases: Structure and Mechanism, *Curr. Opin. Chem. Biol. 3*, 614−622.
11. Crowder, M. W., Wang, Z., Franklin, S. L., Zovinka, E. P., and Benkovic, S. J. (1996) Characterization of the Metal Binding Sites of the β-Lactamase from *Bacteroides fragilis*, *Biochemistry 35*, 12126−12132.
12. Orellano, E. G., Girardini, J. E., Cricco, J. A., Ceccarelli, E. A., and Vila, A. J. (1998) Spectroscopic characterization of a binuclear metal site in *Bacillus cereus* β-lactamase II, *Biochemistry 37*, 10173−10180.
13. Valladares, M. H., Felici, A., Weber, G., Adolph, H. W., Zeppezauer, M., Rossolini, G. M., Amicosante, G., Frere, J. M., and Galleni, M. (1997) Zn(II) Depedence of the *Aeromonas hydrophila* AE036 Metallo-β-Lactamase Activity and Stability, *Biochemistry 36*, 11534−11541.
14. Valladares, M. H., Kiefer, M., Heinz, U., Soto, R. P., Meyer-Klaucke, W., Nolting, H. F., Zeppezauer, M., Galleni, M., Frere, J. M., Rossolini, G. M., Amicosante, G., and Adolph, H. W. (2000) Kinetic and Spectroscopic Characterization of Native and Metal-Substituted β-Lactamase from *Aeromonas hydrophila* AE036, *FEBS Lett. 467*, 221−225.
15. Walsh, T. R., Gamblin, S., Emery, D. C., MacGowan, A. P., and Bennett, P. M. (1996) Enzyme Kinetics and Biochemical Analysis of ImiS, the Metallo-β-lactamase from *Aeromonas sobria* 163a, *J. Antimicrob. Chemother. 37*, 423−431.
16. Crowder, M. W., Walsh, T. R., Banovic, L., Pettit, M., and Spencer, J. (1998) Overexpression, Purification, and Characterization of the Cloned Metallo-β-Lactamase L1 from *Stenotrophomonas maltophilia*, *Antimicrob. Agents Chemother. 42*, 921−926.
17. Ullah, J. H., Walsh, T. R., Taylor, I. A., Emery, D. C., Verma, C. S., Gamblin, S. J., and Spencer, J. (1998) The crystal structure of the L1 metallo-β-lactamase from *Stenotrophomonas maltophilia* at 1.7 angstrom resolution, *J. Mol. Biol. 284*, 125−136.
18. Mercuri, P. S., Bouillenne, F., Boschi, L., Lamotte-Brasseur, J., Amicosante, G., Devreese, B., van Beeumen, J., Frere, J. M., Rossolini, G. M., and Galleni, M. (2001) Biochemical characterization of the FEZ-1 metallo-β-lactamase of *Legionella gormanii* ATCC 33297T produced in *Escherichia coli*, *Antimicrob. Agents Chemother. 45*, 1254−1262.
19. Galleni, M., Lamotte-Brasseur, J., Rossolini, G. M., Spencer, J., Dideberg, O., and Frere, J. M. (2001) Standard Numbering Scheme for Class Bβ-Lactamases, *Antimicrob. Agents Chemother. 45*, 660−663.
20. Boschi, L., Mercuri, P. S., Riccio, M. L., Amicosante, G., Galleni, M., Frere, J. M., and Rossolini, G. M. (2000) The *Legionella (Fluoribacter) gormanii* Metallo-β-Lactamase: A New Member of the Highly Divergent Lineage of Molecular Subclass B3 β-Lactamases, *Antimicrob. Agents Chemother. 44*, 1538−1543.
21. Bounaga, S., Laws, A. P., Galleni, M., and Page, M. I. (1998) The Mechanism of Catalysis and the Inhibition of the *Bacillus cereus* Zinc-Dependent β-Lactamase, *Biochem. J. 331*, 703−711.
22. Bounaga, S., Galleni, M., Laws, A. P., and Page, M. I. (2001) Cysteinyl Peptide Inhibitors of *Bacillus cereus* Zinc β-Lactamase, *Bioorg. Med. Chem. 9*, 503−510.
23. Bush, K., Macalintal, C., Rasmussen, B. A., Lee, V. J., and Yang, Y. (1993) Kinetic Interactions of Tazobactam with β-Lactamases from all Major Structural Classes, *Antimicrob. Agents Chemother. 37*, 851−858.
24. Carenbauer, A. L., Garrity, J. A., Periyannan, G., Yates, R. B., and Crowder, M. W. (2002) Probing Substrate Binding to Metallo-β-Lactamase L1 from *Stenotrophomonas maltophilia* by Using Site-Directed Mutagenesis, *BMC Biochem. 3*, 4−10.
25. de Seny, D., Heinz, U., Wommer, S., Kiefer, M., Meyer-Klaucke, W., Galleni, M., Frere, J. M., Bauer, R., and Adolph, H. W. (2001) Metal ion binding and coordination geometry for wild type and mutants of metallo−β-lactamase from *Bacillus cereus* 569/H/9 (BcII)−A combined thermodynamic, kinetic, and spectroscopic approach, *J. Biol. Chem. 276*, 45065−45078.
26. de Seny, D., Prosperi-Meys, C., Bebrone, C., Rossolini, G. M., Page, M. I., Noel, P., Frere, J. M., and Galleni, M. (2002) Mutational analysis of the two zinc-binding sites of the *Bacillus cereus* 569/H/9 metallo-β-lactamase, *Biochem. J. 363*, 687−696.
27. Felici, A., Amicosante, G., Oratore, A., Strom, R., Ledent, P., Joris, B., Fanuel, L., and Frere, J. M. (1993) An Overview of the Kinetic Parameters of Class B β-Lactamases, *Biochem. J. 291*, 151−155.
28. Goto, M., Takahashi, T., Yamashita, F., Koreeda, A., Mori, H., Ohta, M., and Arakawa, Y. (1997) Inhibition of the Metallo-β-Lactamase Produced from *Serratia marcescens* by Thiol Compounds, *Biol. Pharm. Bull. 20*, 1136−1140.
29. McMannus-Munoz, S., and Crowder, M. W. (1999) Kinetic Mechanism of Metallo-β-Lactamase L1 from *Stenotrophomonas maltophilia*, *Biochemistry 38*, 1547−1553.
30. Payne, D. J., Bateson, J. H., Gasson, B. C., Proctor, D., Khushi, T., Farmer, T. H., Tolson, D. A., Bell, D., Skett, P. W., Marshall, A. C., Reid, R., Ghosez, L., Combret, Y., and Marchand-Brynaert, J. (1997) Inhibition of Metallo-β-Lactamases by a Series of Mercaptoacetic Acid Thiol Ester Derivatives, *Antimicrob. Agents Chemother. 41*, 135−140.
31. Payne, D. J., Bateson, J. H., Gasson, B. C., Khushi, T., Proctor, D., Pearson, S. C., and Reid, R. (1997) Inhibition of Metallo-β-Lactamases by a Series of Thiol Ester Derivatives of Mercaptophenylacetic Acid, *FEMS Microbiol. Lett. 157*, 171−175.
32. Tsang, W. Y., Dhanda, A., Schofield, C. J., Frere, J. M., Galleni, M., and Page, M. I. (2004) The inhibition of metallo-β-lactamase by thioxo- cephalosporin derivatives, *Bioorg. Med. Chem. Lett. 14*, 1737−1739.
33. Carfi, A., Pares, S., Duee, E., Galleni, M., Duez, C., Frere, J. M., and Dideberg, O. (1995) The 3-D Structure of a Zinc Metallo-β-Lactamase from *Bacillus cereus* Reveals a New Type of Protein Fold, *EMBO J. 14*, 4914−4921.
34. Fitzgerald, P. M. D., Wu, J. K., and Toney, J. H. (1998) Unanticipated Inhibition of the Metallo-β-Lactamase from *Bacter-*

oides fragilis by 4-Morpholineethanesulfonic Acid (MES): A Crystallographic Study at 1.85 Å Resolution, *Biochemistry 37*, 6791−6800.
35. Fabiane, S. M., Sohi, M. K., Wan, T., Payne, D. J., Bateson, J. H., Mitchell, T., and Sutton, B. J. (1998) Crystal Structure of the Zinc-Dependent β-Lactamase from *Bacillus cereus* at 1.9 Å Resolution: Binuclear Active Site with Features of a Mononuclear Enzyme, *Biochemistry 37*, 12404−12411.
36. Crowder, M. W., Yang, K. W., Carenbauer, A. L., Periyannan, G., Seifert, M. A., Rude, N. E., and Walsh, T. R. (2001) The Problem of a Solvent Exposable Disulfide when Preparing Co(II)-Substituted Metallo-β-Lactamase L1 from *Stenotrophomonas maltophilia*, *J. Biol. Inorg. Chem. 6*, 91−99.
37. Yanchak, M. P., Taylor, R. A., and Crowder, M. W. (2000) Mutational Analysis of Metallo-β-Lactamase CcrA from *Bacteroides fragilis*, *Biochemistry 39*, 11330−11339.
38. Wang, Z., and Benkovic, S. J. (1998) Purification, Characterization, and Kinetic Studies of Soluble *Bacteroides fragilis* Metallo-β-Lactamase, *J. Biol. Chem. 273*, 22402−22408.
39. Rasia, R. M., and Vila, A. J. (2003) Mechanistic study of the hydrolysis of nitrocefin mediated by *B. cereus* metallo-β-lactamase, *ARKIVOC 3*, 507−516.
40. Garrity, J. D., Carenbauer, A. L., Herron, L. R., and Crowder, M. W. (2004) Metal Binding Asp-120 in Metallo-β-lactamase L1 from *Stenotrophomonas maltophilia* Plays a Crucial Role in Catalysis, *J. Biol. Chem. 279*, 920−927.
41. Dal Peraro, M., Vila, A. J., and Carloni, P. (2003) Protonation state of Asp120 in the binuclear active site of the metallo-β-lactamase from *Bacteroides fragilis*, *Inorg. Chem. 42*, 4245−4247.
42. Diaz, N., Suarez, D., and Merz, K. M. (2000) Zinc Metallo-β-Lactamase from *Bacteroides fragilis*: A Quantum Chemical Study on Model Systems of the Active Site, *J. Am. Chem. Soc. 122*, 4197−4208.
43. Diaz, N., Suarez, D., and Merz, K. M. (2001) Molecular dynamics simulations of the mononuclear zinc-β- lactamase from *Bacillus cereus* complexed with benzylpenicillin and a quantum chemical study of the reaction mechanism, *J. Am. Chem. Soc. 123*, 9867−9879.
44. Prosperi-Meys, C., Wouters, J., Galleni, M., and Lamotte-Brasseur, J. (2001) Substrate binding, and catalytic mechanism of class Bβ-lactamases: a molecular modelling study, *Cell. Mol. Life Sci. 58*, 2136−2143.
45. Salsbury, F. R., Crowley, M. F., and Brooks, C. L. (2001) Modeling of the metallo−β-lactamase from *B-fragilis*: Structural and dynamic effects of inhibitor binding, *Proteins: Struct., Funct., Genet. 44*, 448−459.
46. Suarez, D., and Merz, K. M. (2001) Molecular Dynamics Simulations of the Mononuclear Zinc-β-Lactamase from *Bacillus cereus*, *J. Am. Chem. Soc. 123*, 3759−3770.
47. Suarez, D., Brothers, E. N., and Merz, K. M. (2002) Insights into the structure and dynamics of the dinuclear zinc β-lactamase site from *Bacteroides fragilis*, *Biochemistry 41*, 6615−6630.
48. Suarez, D., Diaz, N., and Merz, K. M. (2002) Molecular dynamics simulations of the dinuclear zinc-β- lactamase from *Bacteroides fragilis* complexed with imipenem, *J. Comput. Chem. 23*, 1587−1600.
49. Walsh, T. R., Neville, W. A., Haran, M. H., Tolson, D., Payne, D. J., Bateson, J. H., MacGowan, A. P., and Bennett, P. M. (1998) Nucleotide and Amino Acid Sequences of the Metallo-β-Lactamase, ImiS, from *Aeromonas veronii bv. sobria*, *Antimicrob. Agents Chemother. 42*, 436−439.
50. Crawford, P. A., Sharma, N., Chandrasekar, S., Sigdel, T., Walsh, T. R., Spencer, J., and Crowder, M. W. (2004) Over-expression, purification, and characterization of metallo-β-lactamase ImiS from *Aeromonas veronii bv. sobria*, *Protein Expression Purif. 36*, 272−279.
51. Yang, K. W., and Crowder, M. W. (2004) Method for removing EDTA from Apo-proteins, *Anal. Biochem. 329*, 342−344.
52. Wang, D. M., and Hanson, G. R. (1995) A New Method for Simulating Randomly Oriented Powder Spectra in Magnetic-Resonance−the Sydney-Opera-House (Sophe) Method, *J. Magn. Reson. Ser. A 117*, 1−8.
53. Bennett, B., and Holz, R. C. (1997) EPR Studies on the Mono- and Dicobalt(II)-Substituted Forms of the Aminopeptidase from *Aeromonas proteolytica*. Insight into the Catalytic Mechanism of Dinuclear Hydrolases, *J. Am. Chem. Soc. 119*, 1923−1933.
54. Wommer, S., Rival, S., Heinz, U., Galleni, M., Frere, J. M., Franceschini, N., Amicosante, G., Rasmussen, B., Bauer, R., and Adolph, H. W. (2002) Substrate-activated zinc binding of metallo-β-lactamases−Physiological importance of the mononuclear enzymes, *J. Biol. Chem. 277*, 24142−24147.
55. Bertini, I., and Luchinat, C. (1984) High-Spin Cobalt(II) as a Probe for the Investigation of Metalloproteins, *Adv. Inorg. Biochem. 6*, 72−111.
56. Banci, L., Bertini, I., Luchinat, C., Piccioli, M., Scozzafava, A., and Turano, P. (1989) Proton NOE studies on dicopper(II) dicobalt(II) superoxide dismutase, *Inorg. Chem. 28*, 4650−4656.
57. Estiu, G. L., Rasia, R. M., Cricco, J. A., Vila, A. J., and Zerner, M. C. (2002) Is there a bridging ligand in metal-substituted zinc β-lactamases? A spectroscopic and theoretical answer., *Int. J. Quantum Chem. 88*, 118−132.
58. Bertini, I., Gerber, M., Lanini, G., Luchinat, C., Maret, W., Rawer, S., and Zeppezauer, M. (1984) ^{1}H NMR Investigation of the Active Site of Cobalt(II)-Substituted Liver Alcohol Dehydrogenase, *J. Am. Chem. Soc. 106*, 1826−1830.
59. Bertini, I., Canti, G., Luchinat, C., and Mani, F. (1981) ^{1}H NMR Spectra of the Coordination Sphere of Cobalt-Substituted Carbonic Anhydrase, *J. Am. Chem. Soc. 103*, 7784−7788.
60. Auld, D. S. (1988) Methods for Metal Substitution, *Methods Enzymol. 158*, 71−79.
61. Hernandez Valladares, M., Kiefer, M., Heinz, U., Soto, R. P., Meyer-Klaucke, W., Nolting, H. F., Zeppezauer, M., Galleni, M., Frère, J. M., Rossolini, G. M., Amicosante, G., and Adolph, H. W. (2000) Kinetic and spectroscopic characterization of native and metal- substituted β-lactamase from *Aeromonas hydrophila* AE036, *FEBS Lett. 467*, 221−225.
62. Garmer, D. R., and Krauss, M. (1993) Ab Initio Quantum Chemical Study of the Cobalt d-d Spectroscopy of Several Substituted Zinc Enzymes, *J. Am. Chem. Soc. 115*, 10247−10257.
63. Dennison, C., and Sato, K. (2004) Paramagnetic ^{1}H NMR Spectrum of the Cobalt(II) Derivative of Spinach Plastocyanin, *Inorg. Chem. 43*, 1502−1510.
64. Salgado, J., Jimenez, H. R., Donaire, A., and Moratal, J. M. (1995) ^{1}H NMR Study of a Cobalt-Substituted Blue Copper Protein: *Pseudomonas aeruginosa* Co(II) Azurin, *Eur. J. Biochem. 231*, 358−369.
65. Vila, A. J., Ramirez, B. E., Di Bilio, A. J., Mizoguchi, T. J., Richards, J. H., and Gray, H. B. (1997) Paramagnetic NMR Spectroscopy of Cobalt(II) and Copper(II) Derivatives of *Pseudomonas aeruginosa* His46Asp Azurin, *Inorg. Chem. 36*, 4567−4570.
66. Huntington, K. M., Bienvenue, D. L., Wei, Y. M., Bennett, B., Holz, R. C., and Pei, D. H. (1999) Slow-binding inhibition of the aminopeptidase from *Aeromonas proteolytica* by peptide thiols: Synthesis and spectroscopic characterization, *Biochemistry 38*, 15587−15596.
67. Bienvenue, D. L., Bennett, B., and Holz, R. C. (2000) Inhibition of the aminopeptidase from *Aeromonas proteolytica* by *L*-leucinethiol: kinetic and spectroscopic characterization of a slow, tight-binding inhibitor-enzyme complex, *J. Inorg. Biochem. 78*, 43−54.
68. Bennett, B. (2002) EPR of Co(II) as a Structural and Mechanistic Probe of Metalloprotein Active Sites: Characterization of an Aminopeptidase, *Curr. Top. Biophys. 26*, 49−57.
69. Vanhove, M., Zakhem, M., Devreese, B., Franceschini, N., Anne, C., Bebrone, C., Amicosante, G., Rossolini, G. M., Van Beeumen, J., Frere, J. M., and Galleni, M. (2003) Role of Cys221 and Asn116 in the zinc-binding sites of the *Aeromonas hydrophila* metallo-β-lactamase, *Cell. Mol. Life Sci. 60*, 2501−2509.
70. Garau, G., Bebrone, C., Anne, C., Galleni, M., Frere, J. M., and Dideberg, O. (2005) A metallo-β-lactamase enzyme in action: crystal structure of the monozinc carbapenemase CphA and its complex with biapenem, *J. Mol. Biol. 345*, 785−795.

BI047463S